Nodeless kagome superconductivity in math xmlns="http://www.w3.org/1998/Math/MathML">mrow>msub>mi>LaRu/mi>mn>3/mn>/msub>msub>mi>Si/mi>mn>2/mn>/msub>/mrow>/math>

C. Mielke, III, Y. Qin, J.-X. Yin, H. Nakamura, D. Das, K. Guo, R. Khasanov, J. Chang, Z. Q. Wang, S. Jia, S. Nakatsuji, A. Amato, H. Luetkens, G. Xu, M. Z. Hasan, and Z. Guguchia

Phys. Rev. Materials **5**, 034803 — Published 29 March 2021

DOI: 10.1103/PhysRevMaterials.5.034803

Nodeless kagome superconductivity in $LaRu_3Si_2$

C. Mielke III,[1,2,*] Y. Qin,[3,*] J.-X. Yin,[4,*] H. Nakamura,[5,*] D. Das,[1] K. Guo,[6,7] R. Khasanov,[1] J. Chang,[2] Z.Q. Wang,[8] S. Jia,[6,7] S. Nakatsuji,[5] A. Amato,[1] H. Luetkens,[1] G. Xu,[3,†] M.Z. Hasan,[4,‡] and Z. Guguchia[1,§]

[1] *Laboratory for Muon Spin Spectroscopy, Paul Scherrer Institute, CH-5232 Villigen PSI, Switzerland*
[2] *Physik-Institut, Universitat Zurich, Winterthurerstrasse 190, CH-8057 Zurich, Switzerland*
[3] *Wuhan National High Magnetic Field Center and School of Physics, Huazhong University of Science and Technology, Wuhan 430074, China*
[4] *Laboratory for Topological Quantum Matter and Spectroscopy, Department of Physics, Princeton University, Princeton, NJ, 08544, USA*
[5] *Institute for Solid State Physics, University of Tokyo, Kashiwa, 277-8581, Japan*
[6] *International Center for Quantum Materials and School of Physics, Peking University, Beijing, China*
[7] *CAS Center for Excellence in Topological Quantum Computation, University of Chinese Academy of Science, Beijing, China*
[8] *Department of Physics, Boston College, Chestnut Hill, MA, USA*

We report muon spin rotation (μSR) experiments together with first-principles calculations on microscopic properties of superconductivity in the kagome superconductor $LaRu_3Si_2$ with $T_c \simeq 7$K. Below T_c, μSR reveals type-II superconductivity with a single s-wave gap, which is robust against hydrostatic pressure up to 2 GPa. We find that the calculated normal state band structure features a kagome flat band and Dirac as well as van Hove points formed by the Ru-dz^2 orbitals near the Fermi level. We also find that electron-phonon coupling alone can only reproduce small fraction of T_c from calculations, which suggests other factors in enhancing T_c such as the correlation effect from the kagome flat band, the van Hove point on the kagome lattice, and high density of states from narrow kagome bands. Our experiments and calculations taken together point to nodeless moderate coupling kagome superconductivity in $LaRu_3Si_2$.

I. INTRODUCTION

Layered systems with highly anisotropic electronic properties have been found to be potential hosts for rich, unconventional and exotic quantum states. The prominent class of layered materials is the kagome-lattice systems [1–7]. Crystalline materials that contain a kagome lattice have attracted considerable attention because of the associated electronic band structure and frustrated antiferromagnetic (AFM) interactions. This band structure reveals a pair of Dirac points similar to those found in graphene, and a dispersionless, flat band that originates from the kinetic frustration associated with the geometry of the kagome lattice. Flat bands are exciting because the associated high density of electronic states hints at possible correlated electronic phases when found close to the Fermi level [8–10]. The possibility to access flat bands and their influence on the physical properties of the system has been studied for about three decades [10–17]. Recently, superconductivity was discovered in bilayer graphene [18] when its individual layers are twisted with respect to each other by a specific angle giving rise to a flat band. Recent Monte Carlo calculations on a two-dimensional system [8] demonstrate that the ground state is a superconductor and find a broad pseudogap regime that exhibits strong pairing fluctuations and even a tendency towards electronic phase separation. Moreover, a square-octagon lattice was theoretically studied in which two perfectly flat bands were found [9] and the calculated superconducting phase diagram was found to have two superconducting domes [9], as observed in several types of unconventional superconductors. Thus, there is a resurgence of interest in flat bands as a means to explore unconventional superconductivity from the experimental front [8, 19, 20].

In this framework, the layered system $LaRu_3Si_2$ [21–25] appears to be a good example of a material hosting both a kagome lattice and superconductivity. The structure of $LaRu_3Si_2$ contains distorted kagome layers of Ru sandwiched between layers of La and layers of Si having a honeycomb structure (see Fig. 1a and b), crystallizing in the $P6_3/m$ space group. The system was shown to be a typical type II superconductor with a SC transition temperature with the onset as high as $\simeq 7$ K [23]. Anomalous properties [25] in the normal and SC states [23] were reported in $LaRu_3Si_2$, such as the deviation of the normal state specific heat from the Debye model, non-mean field like suppression of superconductivity with magnetic field and non-linear field dependence of the induced quasiparticle density of states (DOS). However, for the most part only the critical temperatures and fields have been characterized for the superconducting state of $LaRu_3Si_2$. Thus, thorough and microscopic exploration of superconductivity in $LaRu_3Si_2$ from both experimental and theoretical perspectives are required in order to understand the origin of the relatively high value of the critical temperature.

Here, we combine powerful microscopic probe such as

*These authors contributed equally to the paper.
†Electronic address: gangxu@hust.edu.cn
‡Electronic address: mzhasan@princeton.edu
§Electronic address: zurab.guguchia@psi.ch

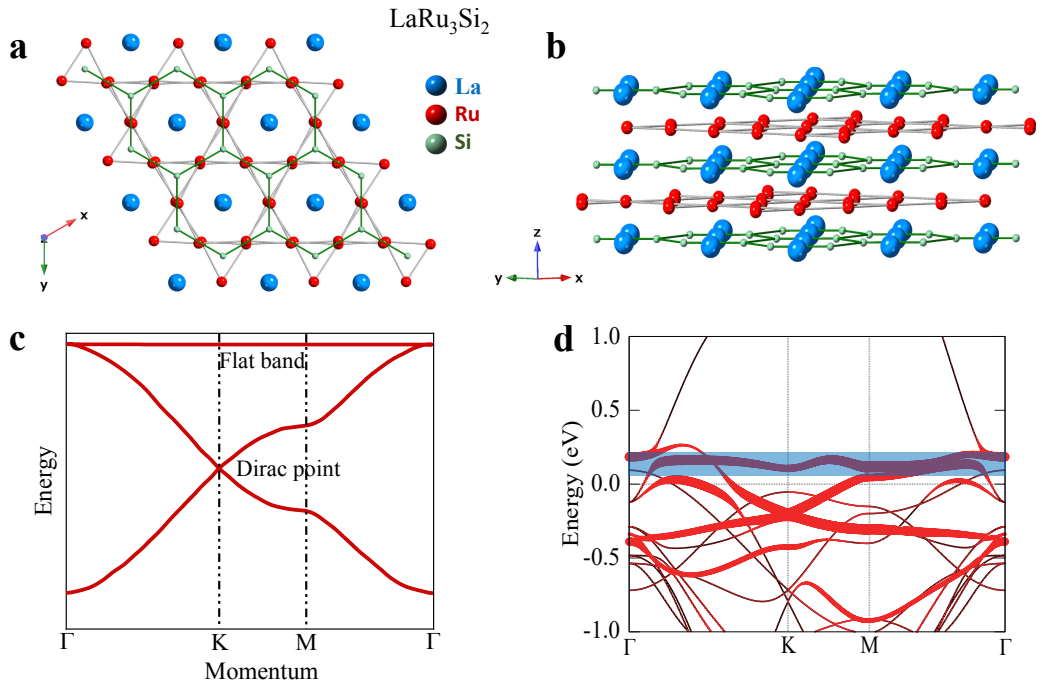

Figure 1: (Color online) Top view (a) and side view (b) of the atomic structure of $LaRu_3Si_2$. The Ru atoms construct a kagome lattice (red middle size circles), while the Si (green small size circles) and La atoms (blue large size circles) form a honeycomb and triangular structure, respectively. (c) Tight-binding band structure of kagome lattice exhibiting two Dirac bands at the K-point and a flat band across the whole Brillouin zone. (d) The band structures (black) and orbital-projected band structure (red) for the Ru-dz^2 orbital without SOC along the high symmetry k-path, presented in conformal kagome BZ. The width of the line indicates the weight of each component. The blue-colored region highlights the manifestation of the kagome flat band.

the muon spin rotation (μSR) [26–29] together with first-principles calculations [30–34] to elucidate the superconductivity in kagome superconductor $LaRu_3Si_2$ with $T_c \simeq 7$ K. We find that the calculated normal state band structure features a kagome flat band, Dirac point and van Hove point formed by the Ru-dz^2 orbitals near the Fermi level. The superfluid density obtained from μSR is best described by the scenario of a single SC gap function without nodes. The measured SC gap value $\Delta = 1.14(1)$ meV yields a BCS ratio $2\Delta/k_BT_c \simeq 4.3$, suggesting that the superconductor $LaRu_3Si_2$ is in the moderate coupling limit. We also find that the electron-phonon coupling alone turns out to be insufficient to reproduce the experimental critical temperature T_c, suggesting kagome-lattice related factors in enhancing T_c.

II. RESULTS AND DISCUSSIONS

The calculated total and projected density of state (DOS) (Figure 2a and supplementary figure S4a), demonstrate that the states at the Fermi level in $LaRu_3Si_2$ are mainly contributed by the Ru 4d electrons. The band structure with the Ru-dz^2 orbital projection is shown in Figure 1d. There are several bands that cross the Fermi level and the complex three dimensional Fermi surfaces (Figure 2b and supplementary figure S4c) are formed in the first Brillouin zone, indicating multi-band physics. Most importantly, in the $k_z = 0$ plane, a flat band of the kagome lattice formed by the Ru-dz^2 orbitals is found 0.1 eV above the Fermi level, highlighted by blue-colored region in Figure 1d. In addition, a Dirac point at the K (K$^{'}$)-point with linear dispersion is found 0.2 eV below the Fermi level. Moreover, the van Hove point on the kagome lattice at M point can be clearly seen in Fig. 1d, which is located even closer to the Fermi energy ($\sim$ 50 meV). Thus, the system $LaRu_3Si_2$ exhibits, around the Fermi level, a typical kagome lattice band structure (see Figure 1c), revealing a Dirac point, the van Hove point and a dispersionless, flat band that originates from the kinetic frustration associated with the geometry of the kagome lattice.

The temperature dependence of electrical resistivity for $LaRu_3Si_2$, depicted in Figure 3a under different applied fields up to 9 T, shows superconductivity with the onset and the midpoint (at 50 % drop of the resistivity) of the transition at 7 K and 6.5 K, respectively. The upper critical magnetic field was estimated to be as high as $\mu_0 H_{c2} = 8.5$ T at $T = 2$ K (see the supplementary Figure S3). In the following, we provide the microscopic details of the superconductivity in this system using μSR.

Figures 3b and c exhibit the transverse field (TF) μSR time spectra for $LaRu_3Si_2$ in an applied magnetic field of

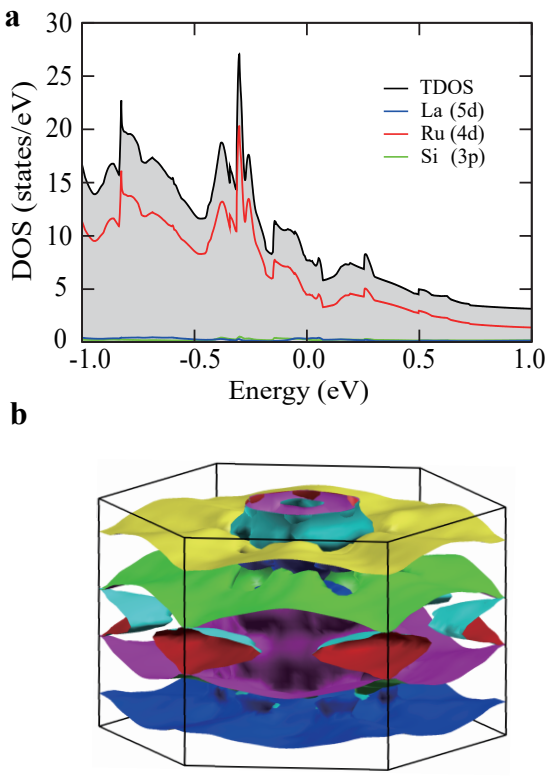

Figure 2: (Color online) (a) The calculated total DOS and projected DOS for the Ru, Si, La atoms in the bulk $LaRu_3Si_2$. (b) Three dimensional Fermi surface of $LaRu_3Si_2$ in the first Brillouin zone.

70 mT, measured at $p = 0$ GPa and maximum applied pressure $p = 1.85$ GPa, respectively. The spectra above (7 K) and below (0.25 K) the SC transition temperature T_c are shown. Above T_c, the oscillations show a small damping due to the random local fields from the nuclear magnetic moments. Below T_c the damping rate strongly increases with decreasing temperature due to the presence of a nonuniform local magnetic field distribution as a result of the formation of a flux-line lattice (FLL) in the SC state. Magnetism, if present in the samples, may enhance the muon spin depolarization rate and falsify the interpretation of the TF-μSR results. Therefore, we have carried out zero-field (ZF)-μSR experiments above and below T_c to search for magnetism (static or weakly fluctuating) in $LaRu_3Si_2$. As shown in Fig. 3d, no sign of either static or fluctuating magnetism could be detected in ZF time spectra down to 0.25 K. The spectra are well described by a Kubo-Toyabe depolarization function [35–37], reflecting the field distribution at the muon site created by the nuclear moments of the sample and the pressure cell. Returning to the discussion of the TF-μSR data, we observe a strong diamagnetic shift of the internal magnetic field $\mu_0 H_{\rm int}$ sensed by the muons below T_c. This is evident in Figure 3e, where we plot the temperature dependence of $\Delta\mu_0 H_{\rm int} = \mu_0(H_{\rm int,SC} - H_{\rm int,NS})$, i.e., the difference between the internal field $\mu_0 H_{\rm int,SC}$ measured in the SC fraction and $\mu_0 H_{\rm int,NS}$ measured in the normal state at $T = 10$ K. The strong diamagnetic shift excludes the occurrence of field induced magnetism in $LaRu_3Si_2$. The absence of magnetism in zero-field or under applied magnetic fields implies that the increase of the TF relaxation rate below T_c is solely arising from the FLL in the superconducting state.

From the TF-μSR time spectra, we determined the Gaussian superconducting relaxation rate $\sigma_{\rm sc}$ (after subtracting the nuclear contribution), which is proportional to the second moment of the field distribution (see Method section). Figure 2f shows $\sigma_{\rm sc}$ as a function of temperature for $LaRu_3Si_2$ at $\mu_0 H = 0.07$ T, recorded for various hydrostatic pressures. Below T_c the relaxation rate $\sigma_{\rm sc}$ starts to increase from zero due to the formation of the FLL. We note that both $\sigma_{\rm sc}$ and T_c stay nearly unchanged under pressure, indicating a robust superconducting state of $LaRu_3Si_2$. At all pressures, $\sigma_{\rm sc}(T)$ shows saturation towards low temperatures.

In order to investigate the symmetry of the SC gap, we note that temperature dependence of the magnetic penetration depth $\lambda(T)$ is related to the relaxation rate $\sigma_{\rm sc}(T)$, in the presence of a perfect triangular vortex lattice by the equation [27]:

$$\frac{\sigma_{sc}(T)}{\gamma_\mu} = 0.06091 \frac{\Phi_0}{\lambda^2_{eff}(T)}, \qquad (1)$$

where γ_μ is the gyromagnetic ratio of the muon, and Φ_0 is the magnetic-flux quantum. Thus, the flat T-dependence of $\sigma_{\rm sc}$ observed at various pressures for low temperatures (see Fig. 3f) is consistent with a nodeless superconductor, in which $\lambda^{-2}_{eff}(T)$ reaches its zero-temperature value exponentially. We note that it is the effective penetration depth λ^{-2}_{eff} (powder average), which we extract from the μSR depolarization rate (Eq. (1)), and this is the one shown in the figures. The magnetic penetration depth is one of the fundamental parameters of a superconductor, since it is related to the superfluid density n_{sc} via $1/\lambda^2_{eff} = \mu_0 e^2 n_{sc}/m^*$ (where m^* is the effective mass and n_s is the SC carrier density). A quantitative analysis of $\lambda_{eff}(T)$ [26, 38–40] is described in the methods section of the supplementary information. The results of this analysis are presented in Fig. 4a-c, where the temperature dependence of λ^{-2}_{eff} for $LaRu_3Si_2$ is plotted at various pressures. The solid and dashed lines represent fits to the data using s-wave and d-wave models, respectively. As seen in Fig. 4, $\lambda_{eff}(T)$ dependence is best described by a momentum independent s-wave model with a gap value of $\Delta = 1.2(1)$ meV and $T_c \simeq 6.5$ K. The effective penetration depth, λ_{eff}, at zero temperature is found to be 240(10) nm. We also tested the power law (1-$(T/T_c)^2$) which has been proposed theoretically [41] for the superfluid density of dirty d-wave superconductors and found it to be inconsistent with the data. The observed single gap superconductivity in this multi-band system implies that the superconducting pairing involves predominately

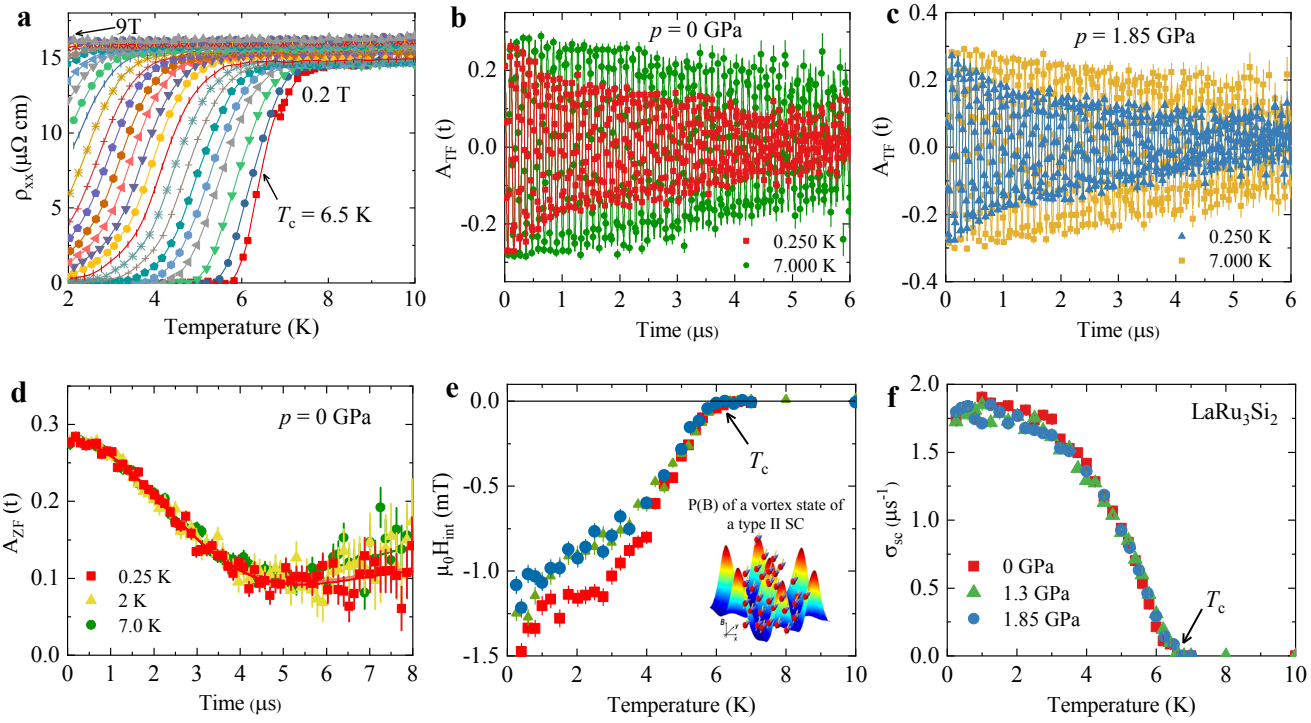

Figure 3: Color online) (a) The temperature dependence of the electrical resistivity for $LaRu_3Si_2$, recorded for various applied magnetic fields. (b-d) Transverse-field (TF) and zero-field (ZF) μSR time spectra for $LaRu_3Si_2$ to probe the SC vortex state and magnetic responses, respectively. The TF spectra are obtained above and below T_c (after field cooling the sample from above T_c): (b) $p = 0$ GPa and (c) $p = 1.85$ GPa. The solid lines in panels a and b represent fits to the data by means of Eq. 1. The dashed lines are a guide to the eye. Inset illustrates how muons, as local probes, sense the inhomogeneous field distribution in the vortex state of type-II superconductor. (d) ZF μSR time spectra for $LaRu_3Si_2$ recorded above and below T_c. The line represents the fit to the data using a standard Kubo-Toyabe depolarization function [35], reflecting the field distribution at the muon site created by the nuclear moments. Temperature dependence of the diamagnetic shift $\Delta\mu_0 H_{\rm int}$ (e) and the muon spin depolarization rate $\sigma_{\rm sc}(T)$ (f), measured at various hydrostatic pressures in an applied magnetic field of $\mu_0 H = 70$ mT. The arrows mark the T_c values.

one band. However, if the inter-band coupling is strong than one may detect single-gap like behavior of the superfluid density even in multigap materials [42].

The ratio of the superconducting gap to T_c for $LaRu_3Si_2$ was estimated to be $(2\Delta/k_B T_c) \simeq 4.3$, which is large. However, it is not out of the limit of conventional superconductivity since similar values for $2\Delta/k_B T_c$ were found for conventional superconductors such as Pb and Hg [43]. On the other hand, a similar ratio can also be expected for Bose Einstein Condensate (BEC)-like picture as pointed out in references [44, 48]. To place this system $LaRu_3Si_2$ in the context of other superconductors, in Fig. 4d we plot the critical temperature T_c against the superfluid density λ_{eff}^{-2}. Most unconventional superconductors have T_c/λ_{eff}^{-2} values of about 0.1-20, whereas all of the conventional BCS superconductors lie on the far right in the plot, with much smaller ratios. In the other words, unconventional superconductors are characterized by a dilute superfluid (low density of Cooper pairs) while conventional BCS superconductors exhibit dense superfluid. Moreover, a linear relationship between T_c and λ_{eff}^{-2} is expected only on the Bose Einstein Condensate (BEC)-like side and is considered a hallmark feature of unconventional superconductivity. We recently showed that the linear correlation is an intrinsic property of the superconductivity in transition metal dichalcogenides [44, 45], whereas the ratio T_c/λ_{eff}^{-2} is lower than the ratio observed in hole-doped cuprates (see Figure 4d). For twisted bilayer graphene [18] the ratio T_c/λ_{eff}^{-2} was found to be even higher than the one for cuprates. For $LaRu_3Si_2$, the ratio is estimated to be $T_c/\lambda_{eff}^{-2} \simeq 0.37$, which is approximately a factor of 15 lower than the one for hole-doped cuprates, but still being far away from conventional phonon-mediated BCS superconductors. Interestingly, the point for $LaRu_3Si_2$ is almost perfectly located on the trend line on which charge density wave superconductors 2H-$NbSe_2$ and 4H-$NbSe_2$ as well as Weyl-superconductor T_d-$MoTe_2$ [44] lie, as shown in Fig. 4d. This finding hints, to some extent, at beyond BCS pairing mechanism in $LaRu_3Si_2$ with a

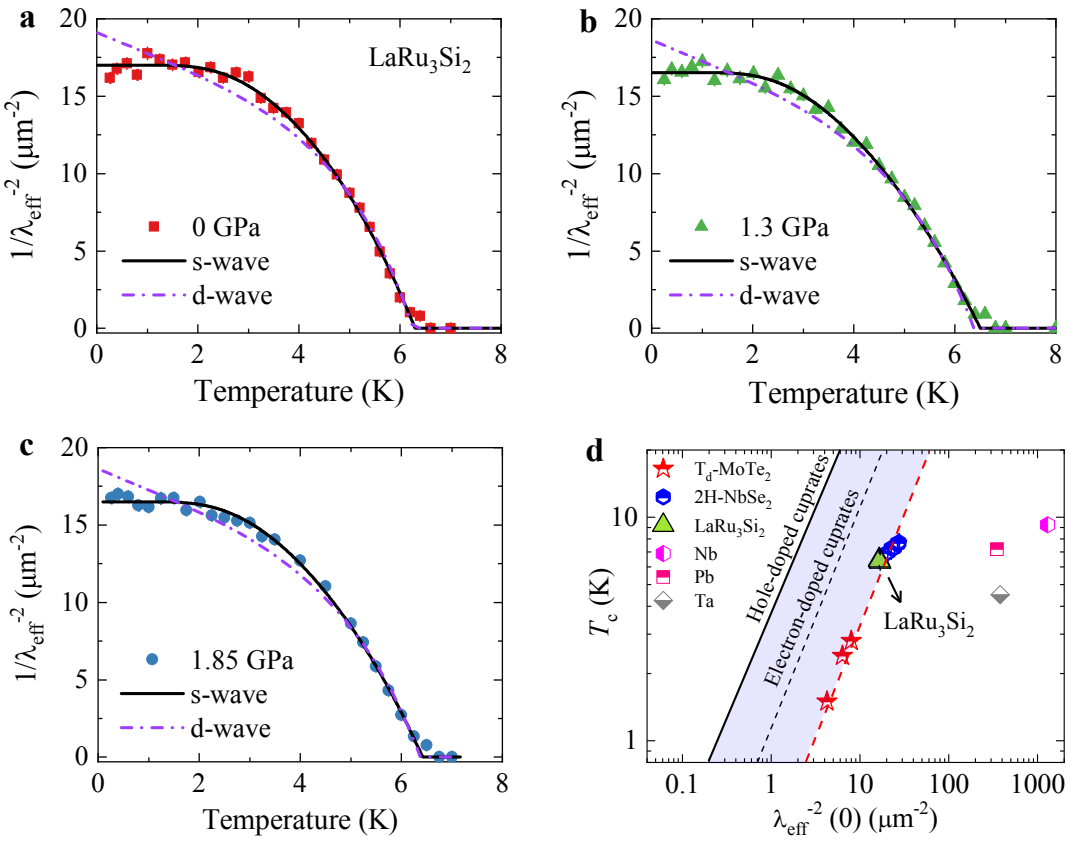

Figure 4: (Color online) The temperature dependence of λ_{eff}^{-2} measured at various applied hydrostatic pressures for $LaRu_3Si_2$: (a) $p = 0$ GPa, (b) 1.3 GPa, and (c) 1.85 GPa. The solid line corresponds to a *s*-wave model and the dashed line represents fitting with a *d*-wave model. (d) A plot of T_c versus the $\lambda_{eff}^{-2}(0)$ obtained from our μSR experiments in $LaRu_3Si_2$. The dashed red line represents the relation obtained for layered transition metal dichalcogenide superconductors T_d-$MoTe_2$ [44] and 2H-$NbSe_2$ [45]. The data are taken at ambient as well as under pressure. The relation observed for underdoped cuprates is also shown (solid line for hole doping [46–49] and the dashed black line for electron doping [50, 51]). The points for various conventional BCS superconductors are also shown.

low density of Cooper pairs and similar electron correlations as in 2H-$NbSe_2$ and T_d-$MoTe_2$, but much weaker electron correlations than in cuprates and twisted bilayer graphene.

Since the present muon spin rotation experiments show direct evidence for the absence of local moments of the Ru atom in $LaRu_3Si_2$, this kagome system is different from high-T_c superconductors or spin liquid compounds. It is rather on the side of itinerant kagome or hexagonal systems such as (Cs,K)V_3Sb_5 [52] or even 2H-$NbSe_2$ [45], where μSR shows the absence of magnetic correlations. On the other hand, the system $LaRu_3Si_2$ does not exhibit a CDW ground state unlike the superconductors (Cs,K)V_3Sb_5 [53]. One possibility is that this system is just somewhat away from CDW order and have higher optimal T_c. The fact that the stability of the crystal structure is obtained with the addition of the Hubbard U (see the supplementary information) suggests proximity of this superconductor $LaRu_3Si_2$ to a CDW, since U opposes the CDW. Pressure independent superfluid density was recently reported for CDW free layered transition metal dichalcogenide system 2M-WS_2 [54], while a large enhancement of λ_{eff}^{-2} was found in CDW superconductor 2H-$NbSe_2$ under pressure when suppressing the CDW order [45]. Thus, the robustness of both T_c and the superfluid density λ_{eff}^{-2} of $LaRu_3Si_2$ to hydrostatic pressure strongly suggests that T_c has the optimal value already at ambient pressure and that the system is away from a competing CDW ground state.

In order to understand the origin of T_c, we compare experimentally measured critical temperatures with those calculated using the McMillan equation [55, 56]. The phonon dispersion for $LaRu_3Si_2$, calculated by the GGA+U method with $U = 1$ eV, is shown in Supplementary Figure S4d. It consists of only the positive frequency modes, and the optimized lattice constants agree very well with the experimental parameters. Based on the phonon dispersion, we calculated the electron-phonon coupling constant $\lambda_{e,ph}$ to be $\simeq 0.45$, indicating only a moderate coupling strength in $LaRu_3Si_2$. For such a low

value of $\lambda_{e,ph}$ the following McMillan equation gives a precise estimate of the electron-phonon interaction induced critical temperature as discussed in Ref. [56]:

$$T_c = \frac{\theta}{1.45} \exp\Big[-\frac{1.04(1+\lambda_{e,ph})}{\lambda_{e,ph} - \mu^*(1+0.62\lambda_{e,ph})}\Big] \quad (2)$$

By using the $\lambda_{e,ph} \simeq 0.45$, Debye temperature $\theta = 280$ K and the Coulomb pseudo potential $\mu^* = 0.12$, the superconducting transition temperature T_c was estimated to be $T_c \simeq 1.2$ K. The calculated value of T_c is obviously much smaller than the experimental value. Since the electron-phonon coupling can reproduce only small fraction of the experimental T_c, other factors in enhancing T_c must be considered. The calculations show the presence of a flat band near the Fermi level, which may enhance correlations and can contribute to the enhancement of T_c in this system. However, the flat band is 100 meV above E_f and it may not have a key role in enhancing T_c. The van Hove point on the kagome lattice at M point, seen in Fig. 1d, is located even closer to the Fermi energy ($\sim$ 50 meV), which can also contribute to the enhancement of T_c. This van Hove point at M is of a similar distance to E_f (below E_f) in KV_3Sb_5, and is what was shown to drive the 2x2 CDW order [53] at much higher temperatures than T_c. Moreover, we find that the whole kagome bands are somewhat narrow ($\sim$ 300 meV), which may also enhance T_c through the overall higher density of states. The narrowness of the kagome bands to be $\sim$ 300 meV may be formally similar to a group of narrow bands, found in twisted bilayer graphene [18].

III. SUMMARY

In summary, we provide the first microscopic investigation of superconductivity in the layered distorted kagome superconductor $LaRu_3Si_2$ with a bulk probe. Specifically, the zero-temperature magnetic penetration depth $\lambda_{eff}(0)$ and the temperature dependence of λ_{eff}^{-2} were studied by means of μSR experiments. The superfluid density is best described by the scenario of a gap function without nodes. Interestingly, the T_c/λ_{eff}^{-2} ratio is far away from those of conventional phonon-mediated BCS superconductors, suggesting that to some extent superconductivity in $LaRu_3Si_2$ is mediated by some pairing mechanism beyond BCS pairing, evidenced by the low density of Cooper pairs. Furthermore, we find the calculated normal state band structure features a kagome flat band, Dirac point and van Hove point formed by the Ru-dz^2 orbitals near the Fermi level. The electron-phonon coupling induced critical temperature T_c, estimated from the phonon dispersion, was found to be much smaller than the experimental value. Thus, the enhancement of T_c in $LaRu_3Si_2$ is attributed to the presence of the flat band and the van Hove point relatively close to the Fermi level as well as to the high density of states from the narrow kagome bands. Our experiments and calculations taken together point to nodeless kagome superconductivity in $LaRu_3Si_2$.

IV. ACKNOWLEDGMENTS

μSR experiments under pressure were performed at the μE1 beamline of the Paul Scherrer Institute (Villigen, Switzerland using the instrument GPD, where an intense high-energy (p_μ = 100 MeV/c) beam of muons is implanted in the sample through the pressure cell. Z.G. thanks Rafael Fernandes for useful discussions. M.Z.H. acknowledges visiting scientist support from IQIM at the California Institute of Technology. Z.Q.W. is supported by DOE grant No. DE-FG02-99ER45747. G. Xu and Y. Qin would like to thank the support by the National Key Research and Development Program of China (2018YFA0307000) and the National Natural Science Foundation of China (11874022).

[1] J-X. Yin, et. al., Giant and anisotropic spin-orbit tunability in a strongly correlated kagome magnet. Nature **562**, 91-95 (2018).
[2] L. Ye, et. al., Massive Dirac fermions in a ferromagnetic kagome metal. Nature **555**, 638-642 (2018).
[3] T.-H. Han, et. al., Fractionalized excitations in the spin-liquid state of a kagome-lattice antiferromagnet. Nature **492**, 406-410 (2012).
[4] Jia-Xin Yin, Songtian S. Zhang, Guoqing Chang, Qi Wang, Stepan Tsirkin, Zurab Guguchia, Biao Lian, Huibin Zhou, Kun Jiang, Ilya Belopolski, Nana Shumiya, Daniel Multer, Maksim Litskevich, Tyler A. Cochran, Hsin Lin, Ziqiang Wang, Titus Neupert, Shuang Jia, Hechang Lei, M. Zahid Hasan. Negative flatband magnetism in a spin-orbit coupled kagome magnet. Nature Physics **15**, 443 (2019).
[5] Z. Guguchia, J. Verezhak, D. Gawryluk, S. S. Tsirkin, J. -X. Yin, I. Belopolski, H. Zhou, G. Simutis, S. -S. Zhang, T. A. Cochran, G. Chang, E. Pomjakushina, L. Keller, Z. Skrzeczkowska, Q. Wang, H. C. Lei, R. Khasanov, A. Amato, S. Jia, T. Neupert, H. Luetkens, M. Z. Hasan. Tunable anomalous Hall conductivity through volume-wise magnetic competition in a topological kagome magnet. Nature Communications **11**, 559 (2020).
[6] O.V. Yazyev, An upside-down magnet. Nature Physics **15**, 424-425(2019).
[7] Nirmal J. Ghimire and Igor I. Mazin, Topology and correlations on the kagome lattice. Nature Materials **19**, 137-138(2020).
[8] J.S. Hofmann, E. Berg, and D. Chowdhury, Superconductivity, pseudogap, and phase separation in topological flat bands. Phys. Rev. B **102**, 201112(R) (2020).

[9] L.H.C.M. Nunes and C.M. Smith, Flat-band superconductivity for tight-binding electrons on a square-octagon lattice. Phys. Rev. B **101**, 224514 (2020).

[10] G.E. Volovik, JETP Lett. **107**, 516 (2018).

[11] T.T. Heikkila, N.B. Kopnin, and G.E. Volovik, JETP Lett. **94**, 233 (2011).

[12] N.B. Kopnin, T.T. Heikkila, and G. E. Volovik, Phys. Rev. B **83**, 220503(R) (2011).

[13] E.H. Lieb, Phys. Rev. Lett. **62**, 1201 (1989).

[14] A. Tanaka and H. Ueda, Phys. Rev. Lett. **90**, 067204 (2003).

[15] K. Noda, A. Koga, N. Kawakami, and T. Pruschke, Phys. Rev. A **80**, 063622 (2009).

[16] A. Julku, S. Peotta, T. I. Vanhala, D.-H. Kim, and P. Torma, Phys. Rev. Lett. **117**, 045303 (2016).

[17] N. Hartman, W.-T. Chiu, and R. T. Scalettar, Phys. Rev. B **93**, 235143 (2016).

[18] Y. Cao, V. Fatemi, A. Demir, S. Fang, S. L. Tomarken, J. Y. Luo, J. D. Sanchez-Yamagishi, K. Watanabe, T. Taniguchi, E. Kaxiras, R. C. Ashoori, and P. Jarillo-Herrero, Nature **556**, 80 (2018).

[19] S. Peotta and P. Torma, Nat. Commun. **6**, 8944 (2015).

[20] S. Sayyad, E.W. Huang, M. Kitatani,M.-S. Vaezi, Z. Nussinov, A. Vaezi, and H. Aoki, Phys. Rev. B **101**, 014501 (2020).

[21] H. Barz, Mater. Res. Bull. PNAS **15**, 1489 (1980).

[22] J. M. Vandenberg and H. Barz, ibid. **15**, 1493 (1980).

[23] Y. Kishimoto, T. Ohno, T. Hihara, K. Sumiyama, G. Ghosh, and L.C. Gupta, Magnetic Susceptibility Study of $LaRu_3Si_2$. J. Phys. Soc. Jpn. **71**, 2035-2038 (2002).

[24] B. Li, S. Li, and H.-H. Wen, Chemical doping effect in the $LaRu_3Si_2$ superconductor with a kagome lattice. Phys. Rev. B **94**, 094523 (2016).

[25] S. Li, B. Zeng, X. Wan, F. Han, J. Tao, H. Yang, Z. Wang, and H.-H. Wen. Anomalous Properties in the Normal and Superconducting States of $LaRu_3Si_2$. Phys. Rev. B **84**, 214527 (2011).

[26] J. E. Sonier, J.H. Brewer, and R.F. Kiefl, μSR studies of the vortex state in type-II superconductors. Rev. Mod. Phys. **72**, 769 (2000).

[27] Brandt, E.H. Flux distribution and penetration depth measured by muon spin rotation in high-T_c superconductors. *Phys. Rev. B* **37**, 2349 (1988).

[28] Z. Guguchia, A. Amato, J. Kang, H. Luetkens, P.K. Biswas, G. Prando, F. von Rohr, Z. Bukowski, A. Shengelaya, H. Keller, E. Morenzoni, R.M. Fernandes, and R. Khasanov, Direct evidence for the emergence of a pressure induced nodal superconducting gap in the iron-based superconductor $Ba_{0.65}Rb_{0.35}Fe_2As_2$. Nature Communications **6**, 8863 (2015).

[29] G.M. Luke, Y. Fudamoto, K.M. Kojima, M.I. Larkin, J. Merrin, B. Nachumi, Y.J. Uemura, Y. Maeno, Z.Q. Mao, Y. Mori, H. Nakamura and M. Sigrist, Time-reversal symmetrybreaking superconductivity in Sr_2RuO_4. Nature **394**, 559 (1998).

[30] G. Kresse and J. Furthmüller, Efficient iterative schemes for ab initio total-energy calculations using a plane-wave basis set. Phys. Rev. B **54**, 11169, (1996).

[31] J. P. Perdew, K. Burke, and M. Ernzerhof, Generalized Gradient Approximation Made Simple. Physical. Review. Letters **77**, 3865, (1996).

[32] V.I. Anisimov, J. Zaanen, and O.K. Andersen, Band theory and Mott insulators: Hubbard U instead of Stoner I. Phys. Rev. B **44**, 943, (1991).

[33] P. Giannozzi, S. De Gironcoli, P. Pavone, and S Baroni, Ab initio calculation of phonon dispersions in semiconductors. Phys. Rev. B **43**, 7231, (1991).

[34] A. Togo, Phonopy, https://atztogo.github.io/phonopy.

[35] R. Kubo and T. Toyabe, Magnetic Resonance and Relaxation (North Holland, Amsterdam, 1967).

[36] R. Khasanov, Z. Guguchia, A. Maisuradze, D. Andreica, M. Elender, A. Raselli, Z. Shermadini, T. Goko, F. Knecht, E. Morenzoni, and A. Amato, High pressure research using muons at the Paul Scherrer Institute. High Pressure Research **36**, 140-166 (2016).

[37] Z. Shermadini, R. Khasanov, M. Elender, G. Simutis, Z. Guguchia, K.V. Kamenev, and A. Amato, A low-background piston-cylinder-type hybrid high pressure cell for muon-spin rotation/relaxation experiments. High Pressure Research, **37(4)**, 449-464 (2017).

[38] Suter, A. and Wojek, B.M. *Physics Procedia* **30**, 69 (2012).
The fitting of the T-dependence of the penetration depth with α model was performed using the additional library BMW developped by B.M. Wojek.

[39] Tinkham, M. Introduction to Superconductivity, *Krieger Publishing Company*, *Malabar*, *Florida*, 1975.

[40] Carrington, A. and Manzano, F. Magnetic penetration depth of MgB_2. *Physica C* **385**, 205 (2003).

[41] P.J. Hirschfeld, W.O. Putikka, and D.J. Scalapino, d-wave Model for Microwave Response of High-T_c Superconductors. Phys. Rev. B **50**, 10250 (1994).

[42] R. Gupta, C. Lohnert, C. Wang, D. Johrendt, H. Luetkens, S. Malick, T. Shiroka, Z. Hossain, and R. Khasanov. Isotropic s-wave superconductivity in the noncentrosymmetric charge density wave superconductor $SrPt_2As_2$. Phys. Rev. B 102, 144515 (2020).

[43] G.W. Webb, F. Marsiglio, and J.E. Hirsch, Superconductivity in the elements, alloys and simple compounds. Physica C **514**, 17 (2015).

[44] Z. Guguchia, F. von Rohr, Z. Shermadini, A. T. Lee, S. Banerjee, A. R. Wieteska, C. A. Marianetti, B. A. Frandsen, H. Luetkens, Z. Gong, S. C. Cheung, C. Baines, A. Shengelaya, G. Taniashvili, A. N. Pasupathy, E. Morenzoni, S. J. L. Billinge, A. Amato, R. J. Cava, R. Khasanov, Y. J. Uemura, Signatures of the topological s^{+-} superconducting order parameter in the type-II Weyl semimetal T_d-$MoTe_2$. Nature Communications **8**, 1082 (2017).

[45] F. O. von Rohr, J.-C. Orain, R. Khasanov, C. Witteveen, Z. Shermadini, A. Nikitin, J. Chang, A. R. Wieteska, A. N. Pasupathy, M. Z. Hasan, A. Amato, H. Luetkens, Y. J. Uemura, Z. Guguchia, Unconventional Scaling of the Superfluid Density with the Critical Temperature in Transition Metal Dichalcogenides. Science Advances 5(11), eaav8465 (2019).

[46] Y.J. Uemura et. al., Phys. Rev. Lett. **62**, 2317 (1989).

[47] Y.J. Uemura et. al., Nature **352**, 605 (1991).

[48] Y.J. Uemura et. al., Basic Similarities among Cuprate, Bismuthate, Organic, Chevrel Phase, and Heavy-Fermion Superconductors Shown by Penetration Depth Measurements. Phys. Rev. Lett. **66**, 2665 (1991).

[49] Y.J. Uemura et. al., Condensation, excitation, pairing, and superfluid density in high-Tc superconductors: the magnetic resonance mode as a roton analogue and a possible spin-mediated pairing, J. Phys.: Condens. Matter

16, S4515-S4540 (2004).

[50] H. Luetkens, H.-H. Klauss, M. Kraken, F.J. Litterst, T. Dellmann, R. Klingeler, C. Hess, R. Khasanov, A. Amato, C. Baines, M. Kosmala, O.J. Schumann, M. Braden, J. Hamann-Borrero, N. Leps, A. Kondrat, G. Behr, J. Werner, and B. Büchner, Nature Materials **8**, 305 (2009).

[51] A. Shengelaya, R. Khasanov, D.G. Eshchenko, D. Di Castro, I.M. Savic, M.S. Park, K.H. Him, Sung-IK Lee, K.A. Müller, and H. Keller, Phys. Rev. Lett. **94**, 127001 (2005).

[52] Eric M. Kenney et al. Absence of local moments in the kagome metal KV_3Sb_5 as determined by muon spin spectroscopy. Preprint at arXiv:2012.04737 (2020).

[53] Y.-X. Jiang, J.-X. Yin, M. Denner, N. Shumiya, B.R. Ortiz, J. He, X. Liu, S.S. Zhang, G. Chang, I. Belopolski, Q. Zhang, S. Hossain, T.A. Cochran, D. Multer, M. Litskevich, Z.-J. Cheng, X.P. Yang, Z. Guguchia, G. Xu, Z. Wang, T. Neupert, S.D. Wilson, and M.Z. Hasan. Discovery of topological charge density wave in kagome superconductor KV_3Sb_5. Preprint at arXiv:

[54] Guguchia Z, Gawryluk DJ, Brzezinska M, Tsirkin SS, Khasanov R, Pomjakushina E, von Rohr FO, Verezhak JAT, Hasan MZ, Neupert T, Luetkens H and Amato A, Nodeless superconductivity and its evolution with pressure in the layered dirac semimetal 2M-WS_2. NPJ Quantum Materials **4**, 50 (2019).

[55] W.L. McMillan, Transition Temperature of Strong-Coupled Superconductors. Phys. Rev. **167**, 331 (1968).

[56] J.P. Carbotte. Properties of boson-exchange superconductors. Reviews of Modern Physics **62**, 1027 (1990).